

SonicSieve: Bringing Directional Speech Extraction to Smartphones Using Acoustic Microstructures

Kuang Yuan*
Carnegie Mellon University
kuangy@andrew.cmu.edu

Yifeng Wang*
Carnegie Mellon University
yifengw3@andrew.cmu.edu

Xiyuxing Zhang*
Carnegie Mellon University
Tsinghua University
xiyuxinz@andrew.cmu.edu

Chengyi Shen
Carnegie Mellon University
Zhejiang University
chengyis@andrew.cmu.edu

Swarun Kumar
Carnegie Mellon University
swarun@cmu.edu

Justin Chan
Carnegie Mellon University
justinchan@cmu.edu

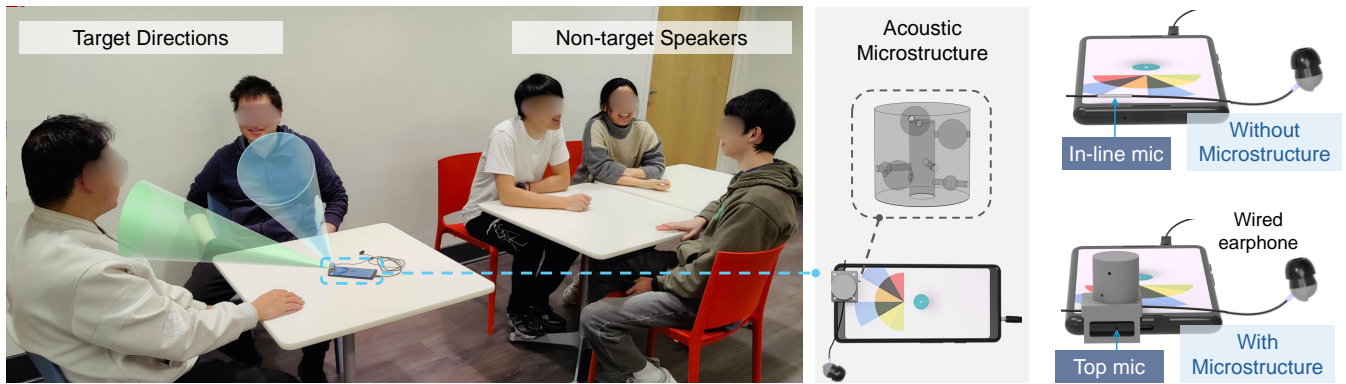


Figure 1: *SonicSieve* enables directional speech extraction on smartphones using a lightweight, passive acoustic microstructure. (Left) Our system leverages the distinct spatial cues created by the 3D-printed microstructure with a real-time neural network to intelligently amplify speech from target directions while attenuating others. (Right) Our design attaches to the in-line microphone of low-cost earphones which can be plugged into a smartphone. The system records sound mixtures from the in-line and top microphone which are used by the neural network to generalize across different sound sources and environments.

ABSTRACT

Imagine placing your smartphone on a table in a noisy restaurant and clearly capturing the voices of friends seated around you, or recording a lecturer’s voice with clarity in a reverberant auditorium. We introduce *SonicSieve*, the first intelligent directional speech extraction system for smartphones using a bio-inspired acoustic microstructure. Our passive design embeds directional cues onto incoming speech without any additional electronics. It attaches to the in-line mic of low-cost wired earphones which can be attached to smartphones. We present an end-to-end neural network that processes the raw audio mixtures in real-time on mobile devices. Our results show that *SonicSieve* achieves a signal quality improvement of 5.0 dB when focusing on a 30° angular region. Additionally, the performance of our system based on only two microphones exceeds that of conventional 5-microphone arrays.

1 INTRODUCTION

Here, we ask the question: *Can we enable directional speech extraction on smartphones?* A positive answer can enable smartphones

to intelligently amplify target speakers and suppress unwanted interference. Imagine having a meeting in a noisy restaurant, and you only want to capture the speech of colleagues at your table for clear meeting notes and to remotely stream to other colleagues back at the office (Fig. 1). Or imagine being a student in a classroom and you want to record the sound of the lecturer without needing a wearable microphone or a dedicated setup.

While rich prior work [11, 23, 29, 36, 45, 50, 58, 59, 64, 70] on intelligent sensing for audio and speech using spatial information exist, they usually rely on arrays of microphones and estimate spatial cues of sounds by analyzing differences in arrival time and sound intensity across the microphones. Although microphone arrays have proliferated across various computing devices from smart speakers and smart glasses to AR/VR headsets, smartphones often contain only two microphones and remain largely unaware of the spatial richness of sound. Additionally, smartphones do not natively support external microphone arrays. While directional microphones exist, they only filter sound from a single, fixed direction, and don’t provide multi-directional separation.

We present *SonicSieve*, the first intelligent directional speech extraction system on smartphones that uses a bio-inspired acoustic

*Co-primary authors

microstructure to embed distinct directional cues into incoming speech sounds from different angles. Our design is inspired by the directional hearing mechanisms found in nature. While human ears function like a two-microphone array, they are able to achieve directional hearing by leveraging spatial cues from the interaction of sound with the structure of the head and pinna [8]. We build on this idea and design a lightweight, miniature 3D-printed cylinder patterned with coded holes that are designed to diffract incoming speech, and create a set of virtual sound sources. The resulting interference patterns form a distinct acoustic signature that changes depending on the direction of a sound, effectively embedding spatial information into the signal.

Our microstructure attaches to the in-line microphone of low-cost wired earbuds, which can be plugged into a smartphone. The system captures audio mixtures using both the in-line microphone and the smartphone’s co-located built-in top microphone, which serves as a reference (Fig. 1) and enables the system to function reliably across diverse sound sources. A real-time neural network running on the smartphone processes these audio mixtures, allowing users to directionally filter speech from different angular sectors. We also design a smartphone user interface that lets users divide the surrounding space into a semicircular region with six 30° sectors. Users can select one or multiple sectors simultaneously, enabling functionality in multi-speaker scenarios (Fig. 13) such as transcribing presentations with multiple speakers or conducting remote meetings in noisy environments like a park.

We build our end-to-end system on a smartphone with a low-cost wired earphone and a 3D-printed microstructure. Our results are as follows:

- Our system achieves a 5.0 dB Scale-Invariant Signal-to-Distortion Ratio (SI-SDR) improvement when focusing on a 30° sector for directional speech extraction, which significantly outperforms the baseline system without microstructure.
- Our system demonstrates generalizable performance across 9 locations in 3 rooms.
- Our average model inference time to process an 8 ms audio chunk is 7.12 ms and 4.46 ms on the Motorola Edge and Google Pixel 7 respectively, demonstrating real-time processing capability.
- Our user study with 20 participants rating 720 audio clips in total shows our system achieve a higher mean opinion score than a system based on a 5-channel microphone array.

We will open source our microstructure design, code, and datasets, which can democratize directional speech extraction capabilities and make it available to the public.

2 RELATED WORK

To the best of our knowledge, no prior work has explored the use of acoustic microstructures to enable directional speech extraction on smartphones. Below we describe work related to acoustic microstructures, spatial sensing, and AI-enabled acoustic systems. **Acoustic sensing using microstructures.** Acoustic microstructures have been designed for a variety of applications, including spatial sensing [5, 20], sound absorption [4, 18], acoustic filtering [32], and biometric identification [69]. Owlet [20] designed a 3D-printed microstructure that embedded directional cues into

incoming sounds, enabling direction-of-arrival (DoA) estimation and sound localization. SPiDR [5] extended this design by using microstructures to project and capture spatially coded signals to generate depth maps of nearby objects. EarCase [34] adapted microstructures for smartphones, embedding them into a custom case for DoA estimation. However, its design required a new custom case for each device, limiting its ability to scale across multiple phone models. Our work differs in two key ways. First, our microstructure is designed for low-cost wired earphones, and is compatible with different smartphones. Second, our work is focused on directional speech extraction by leveraging spatial cues to selectively amplify and suppress speech based on their direction. This enables a broader set of spatial audio interactions beyond what is achievable through DoA alone.

Directional speech extraction. Directional speech extraction is the task of isolating speech from a spatial region that is fixed or adjustable [36]. Prior work [36] explicitly relies on DoA information derived from 8-channel microphone arrays, and does not focus on smartphones. Related approaches [29, 70] explore two- or three-microphone configurations found on some smartphones. However, the spatial cues provided by these configurations are fundamentally limited by both the small number of microphones and their suboptimal placement for spatial sensing tasks. In contrast to these works, we present an acoustic microstructure design which is optimized to enhance the diversity of spatial cues for speech signals. Our system does not require explicit DoA estimation, instead it takes the raw audio mixture as input, and uses an end-to-end network to implicitly infer spatial and acoustic cues, enabling real-time directional speech extraction on smartphones.

Beamforming using statistical algorithms. Traditional beamforming techniques are typically based on statistical algorithms, including non-adaptive approaches such as Bartlett (delay-and-sum) and superdirective beamformers, as well as adaptive methods like minimum-variant distortionless-response (MVDR), and linearly constrained minimum variance (LCMV). However, these algorithms are designed for conventional microphone arrays with fixed and often uniform geometries, and do not account for the complex direction-dependent transformations introduced by acoustic microstructures. As a result, they cannot be directly applied to microstructure-enabled systems like ours, where spatial cues arise not only from microphone placement but also from the physical design of the structure. Moreover, statistical beamformers are limited to capturing spatial cues, and lack the ability to model acoustic cues as neural beamformers do.

Neural beamformers. Prior work on neural beamformers have leveraged LSTM networks [12, 22], but are non-causal and are intended to support full-length audio inputs. Subsequent works [26, 42] introduced causal models that support online processing, but are not real-time. More recent work [56, 57] has focused on designing causal real-time neural beamformers focused on directional hearing for AR headsets, smart glasses, and custom headphones equipped with four or more microphones that provide spatial cues. In contrast, we present a real-time neural network that can process the spatial and acoustic cues of audio that has been filtered by a microstructure, and use this for the task of directional speech extraction.

AI-enabled spatial sensing systems. These systems have focused on speech enhancement [10, 38], sound localization [35, 46],

subject-aware sound classification [61, 75, 76] and speech separation [27, 62]. Recent works have leveraged spatial information to enable new capabilities on smart devices. ClearBuds [10] leverages the placement of wireless earbuds to enable real-time speech enhancement for telephony applications. Cone of Silence [27] extracts speech from multiple target speakers at different locations. Sound Bubble [11] isolates audio within a defined bubble radius, suppressing sound from outside. ReZero [23] extracts all sounds within a user-defined spatial region—angular, spherical, or conical. However, these systems require either a fixed-wearable device like earbuds [9], large microphone arrays with at least six elements, or are not designed for causal, real-time use. In contrast, our work targets directional speech extraction in ad hoc scenarios such as meetings, where the positions of target speakers are unknown in advance. Additionally, we focus on smartphones, which, unlike microphone arrays, are mobile devices that people carry throughout the day.

Spatial sensing on smartphones. Prior work has focused on estimating DoA [30, 52, 77], and beamforming [21] on smartphones using statistical algorithms and neural networks. However, the performance of these systems is fundamentally limited by the limited number of microphones. Ad hoc microphone arrays composed of smartphones have also been proposed for spatial sensing. These systems emulate larger arrays by synchronizing multiple devices. However, they rely on complex synchronization protocols [47] such as aligning smartphone CPU clocks using WiFi beacon timestamps, synchronizing audio I/O clocks through a backend server, or using time-of-arrival techniques [33, 40], which can make deployment in real-world scenarios challenging.

3 SONIC SIEVE

Our system has three main components which we describe below:

- *Acoustic microstructure for speech on smartphones.* We present a compact acoustic microstructure that enables directional speech filtering by creating spatial cues detectable by microphones. Our design attaches to the in-line microphone of low-cost wired earbuds which can be plugged into smartphones. It is easily fabricated using standard 3D printing techniques and generalizes across different sound signals and environments. Our design is optimized for spatial diversity while remaining pocket-sized.
- *Real-time directional speech extraction network.* A directional hearing algorithm is required to extract and interpret the spatial cues from the microstructure. A challenge however with conventional beamformers using signal processing or neural networks is that they are typically designed for uniform microphone array geometries. In contrast, our microstructure introduces spatial diversity through holes that act as virtual sound sources, and produces a complex multipath profile that deviates from these assumptions. We design a real-time neural network that learns the spatial and acoustic cues introduced by the microstructure to simultaneously extract speech from multiple selected directions. This enables multi-speaker transcription in scenarios such as interviews and group discussions.
- *Real-world dataset.* Acoustic and spatial cues signatures learned in one environment may not generalize well to others, as variations in acoustic properties, such as reverberation [67], can distort

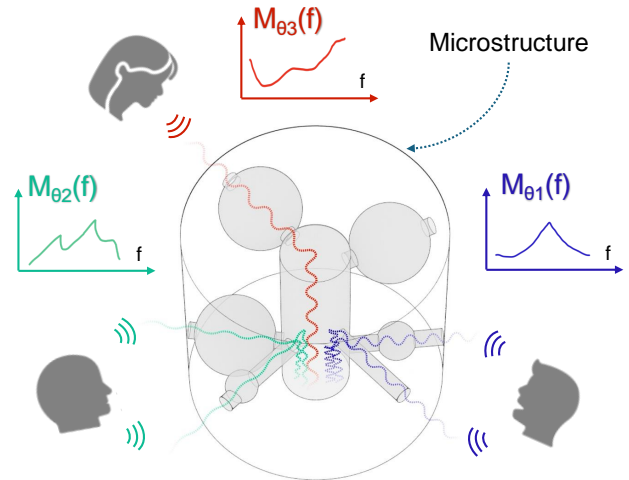


Figure 2: Acoustic microstructure: Principle of operation. The structural elements of the microstructure (holes, tubes, and resonators) form a complex multipath environment that creates variations to incoming acoustic signals based on their direction of arrival.

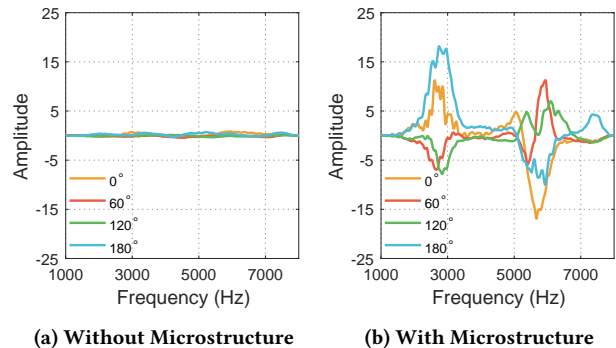


Figure 3: Frequency response ($M_\theta(f)$) at the microphone without and with microstructure for incoming sound signals at different angles of arrival. The plot shows that the microstructure creates greater variation across different angles, which can be leveraged for more effective directional hearing.

the spatial cues encoded by the microstructure. To enable robust performance across different environments, we construct a diverse training dataset that captures the variability encountered in real-world acoustic environments. This dataset is designed to enable generalization across different spaces, speaker configurations, and background noise conditions.

3.1 Speech-aware acoustic microstructure for smartphones

In single-microphone devices, determining the direction of a sound source is difficult as recordings from different angles are similar [43]. While reflections caused by reflectors in the room can encode information about the sound source direction, these cues are specific to

one environment and do not generalize [2, 3]. Microphone arrays can estimate the direction of a sound source by analyzing differences in time and amplitude across multiple microphones, with accuracy improving as microphone count increases [6, 13].

Interestingly, while traditional two-microphone arrays can only localize along one axis with spatial ambiguities [16, 19], humans can localize sound effectively with just two ears [53]. This is due to the geometry of the head and ears which create distinctive reflecting and scattering effects that vary with sound angle [68]. Such a principle is common in nature’s directional hearing system, like asymmetric owl ears [14]. This capability stems from the complex geometry of the head and outer ears, which creates distinctive reflecting and scattering effects that vary with sound angle [68]. This principle appears throughout nature’s directional hearing systems, like the asymmetric ear structures of owls that enable their exceptional sound localization abilities [14]. We take inspiration from this phenomena and aim to create an acoustic microstructure that embeds direction-dependent spatial cues through similar physical effects.

3.1.1 Microstructure Design. We build on top of prior designs [20] consisting of a hollowed-out cylinder that encases a microphone. Below we describe our methodology for selecting key design properties of our microstructure.

- (1) *Surface holes* with ~ 1 mm diameter on the exterior are smaller than speech sound wavelengths, causing incoming sounds to bend (diffract) and create complex direction-dependent sound patterns inside the structure [41].
- (2) *Capillary tubes* connect these holes to the interior, with varying lengths and shapes that modify how sound waves travel through them [39], creating unique phase patterns for sounds from different directions [51].
- (3) *Helmholtz resonators* are small spheres placed along the tubes that act like tiny musical instruments. Each resonator selectively amplifies different frequency bands [49, 72], and enhances the spatial diversity of the resulting acoustic signatures.

Specifically, for a sound source arriving at the microstructure from a relative angle θ and propagating through the internal structure, the microstructure applies a direction-specific filter $M_\theta(f)$ to the sound where f is the frequency (Fig. 2). We show in Fig. 3 the direction-specific filter $M_\theta(f)$ at four different angles without and with the microstructure. The plot shows that the microstructure introduces substantially greater variation across different directions of arrival, and these spatial cues can be used to build a better directional speech extraction network.

Given the microstructure design, our next goal is to estimate such a directional signature $M_\theta(f)$ from the received signal and leverage it to enhance the speech extraction network.

Generalizing across sound sources and environments. In our discussion thus far, we have focused on how the microstructure embeds direction-specific cues onto the signal. In practice, the signal at the microphone is also affected by two other factors: the sound source $S(f)$ and the multipath environment effect $H(f)$ [20, 73], and the received signal at the microphone combines these effects as:

$$R(f) = S(f)H(f)M_\theta(f) \quad (1)$$

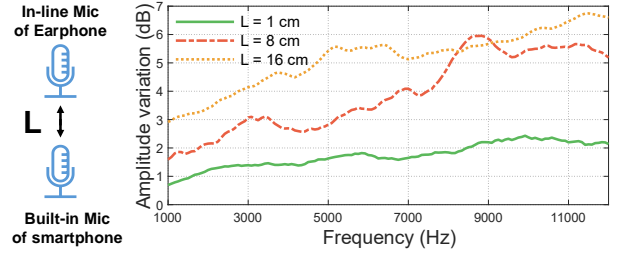


Figure 4: Effect of separation between earphone’s in-line mic and phone’s top mic on spectral variation. We compute the ratio of the received signals at the two microphones ($H_{ratio}(f)$) and estimate the variation across environments (lower is better). When the mics are closely spaced, there is less spectral variation.

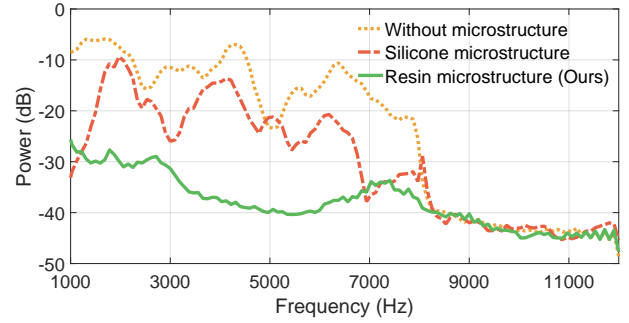


Figure 5: Effect of microstructure material (without holes) on acoustic attenuation. The resin material effectively attenuates sound and ensures that it primarily travels through the microstructure’s holes, rather than its walls.

If the source $S(f)$ is pre-defined and the environmental reflection $H(f)$ is measured beforehand, we can obtain the microstructure’s direction filter by simply canceling their effects through division in the frequency domain (i.e. $M_\theta(f) = \frac{R(f)}{S(f)H(f)}$). However, in practice we cannot know the source signal or the environmental reflection.

To eliminate such source and environment dependency, we incorporate a secondary reference microphone placed outside the microstructure (the built-in microphone on the smartphone). The reference microphone records the sound unmodified by the microstructure simultaneously. The received signal can be denoted as:

$$R_{ref}(f) = S(f)H'(f) \quad (2)$$

We note that the corresponding environment reflection $H'(f)$ differs slightly from $H(f)$ as the reference microphone is not positioned at exactly the same location as the microphone inside the microstructure. To isolate the effect of microstructure, we divide the signal received by the main inside microphone and the reference microphone:

$$\frac{R(f)}{R_{ref}(f)} = \frac{H(f)}{H'(f)} M_\theta(f) = H_{ratio}(f) M_\theta(f) \quad (3)$$

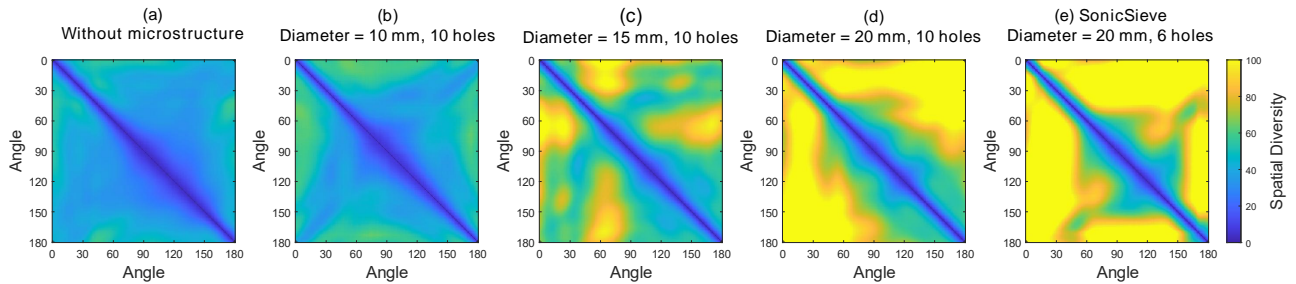


Figure 6: A comparison of spatial diversity across different microstructure designs of varied diameter and hole number. Spatial diversity is computed across angles in a semicircle.

In this way, although the source effect is eliminated, the impact of environmental factors H_{ratio} is not completely removed. To minimize the residual effect of the environmental reflections, we position the reference microphone as close as possible to the microstructure. This proximity minimizes path differences between the two microphones, ensuring that sound waves encounter similar environmental reflections before reaching either microphone, thereby reducing the variation in $H_{ratio}(f)$.

We investigate this empirically and perform a benchmark experiment by placing the in-line mic of the earphone and the built-in top mic of the smartphone at different separation distances and measure the $H_{ratio}(f)$ in 160 locations in total across 4 different environments. Our results shown in Fig. 4 demonstrate that the amplitude variation of $H_{ratio}(f)$ increases with microphone separation. At 1 cm separation, variations remain below 2.2 dB across frequencies, while at 16 cm, variations exceed 6 dB at higher frequencies. Based on this information, our prototype is designed so that the in-line microphone is within 1 cm of the smartphone’s built-in top mic.

3.1.2 Optimizing the microstructure design. Next, we detail key design parameters of the microstructure and their impact on system performance. We then outline our approach for selecting these parameters in the final design. Our goal in optimizing the microstructure is to maximize spatial diversity, in other words, the variation in frequency responses for sound arriving from different directions. To do this, we design a structure that creates unique directional acoustic signatures through three distinct structural elements:

Material Selection. Our goal in selecting a material for the microstructure is to maximize attenuation of incoming sound, ensuring that sound primarily travels through the holes and diffracts as a virtual sound source rather than passing through the walls. To evaluate this, we transmit a 1–8 kHz chirp, covering the frequency range important for understanding human speech [31]—at a sound level of 70 dBA which is on the order of normal conversation. We measure and plot the frequency response at the microphone in three scenarios: without the microstructure, with a silicone microstructure, and with a resin microstructure (Fig. 5). The resin microstructure, which we use in our final design, achieves an average sound reduction of 33 dB across the tested frequencies, outperforming the silicone microstructure, which achieves a reduction of 17 dB.

Microstructure diameter. We measure how the diameter of the microstructure affects its spatial diversity. We measure the overall spatial diversity by calculating $\|M_{\theta_1}(f) - M_{\theta_2}(f)\|_2$ for angle range from 0° to 180° with 1° resolution for all pairwise angles. We varied the microstructure diameter across 10, 15, and 20 mm while measuring spatial diversity, as shown in Fig. 6 (b–d). The plot shows that increasing the diameter leads to greater spatial diversity. However, this improvement comes with a tradeoff: larger microstructures can obstruct the smartphone screen, potentially hindering usability. In our design, we selected a 20 mm diameter as a balance between increased spatial diversity and user experience. **Number of surface holes.** We examine the effect of the number of surface holes on spatial diversity. With only a single hole, directional sensitivity is limited as sounds arriving from directions other than the hole are largely attenuated by the microstructure and cannot be reliably distinguished. On the other hand, if the structure has too many holes, it behaves similarly to having no microstructure at all, with little spatial diversity. We compare the spatial diversity achieved with 6 holes (Fig. 6e) versus 10 holes (Fig. 6d). Empirically, we observe that the configuration with 6 holes provides greater spatial diversity than the 10-hole design, and we select 6 for our final design.

3.1.3 Attaching the microstructure to smartphones. Finally, we describe how the acoustic microstructure is coupled to the in-line microphone of standard earphones. We note that this design choice allows the microstructure to be physically connected to any device with an audio jack, eliminating the need for custom, device-specific cases or attachments. The final design consists of two main components: the top part houses the optimized microstructure, while the bottom part serves as a holder that attaches to the smart device. A silicone washer is placed at the interface between the two components to minimize sound leakage.

3.2 Directional speech extraction network

As described in Sec. 3.1, our approach encodes direction-specific features in the signal recorded by the microphone inside the microstructure (in-line mic at earphone), while capturing an unmodified reference signal using a co-located external microphone (built-in top mic at smartphone). By calculating the ratio between these two signals (Eq. 3), we can extract direction-specific features when a single sound source is present. Although real-world acoustic environments are considerably more complex with multiple sound

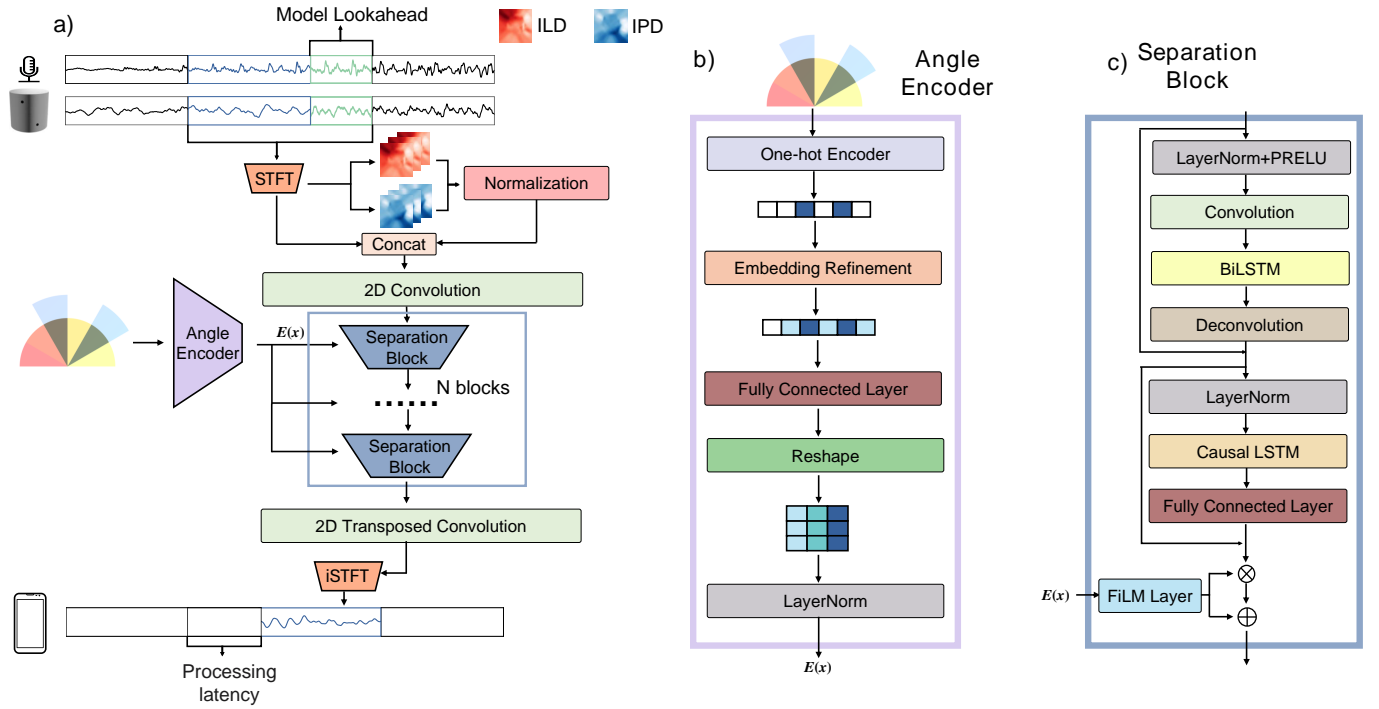


Figure 7: Real-time directional speech extraction network architecture. (a) Audio from the reference mic and the microstructure mic is converted to a spectrogram, ILD/IPD features are extracted, and directional separation is performed based on a user-selected spatial sector. The transformed spectrogram is then converted back to the time domain. (b) The angle encoder converts the selected sector into a normalized embedding for conditioning the separation blocks. (c) Separation blocks use this angle-conditioned embedding to apply directional masking on the spectrogram.

sources, this fundamental principle remains effective for extracting spatial features. These features, combined with the raw two-channel recordings, provide our neural network with the necessary information to perform directional speech separation.

To support applications such as audio live streaming via existing communication protocols, real-time processing capability on smartphones is essential. To achieve this, we start our neural network design from a state-of-the-art real-time sound extraction network [11] and adapt it to our of angular-based directional speech extraction.

Pre-processing Module. Our system takes a 2-channel audio input represented as $x = [x_1, x_2]^T \in R^{2 \times T}$, where x_1 and x_2 correspond to the reference microphone and in-microstructure microphone signals respectively, with T representing the total audio sample length. To accommodate model lookahead requirements, we reshape the input with zero padding to $x \in R^{2 \times (T+\sigma)}$, where σ is the lookahead sample count.

We implement a learnable Short-Time Fourier Transform (STFT) encoder that provides a sufficiently large encoder window size, enhancing model stability across different reverberation environments [15]. After applying the STFT encoder with discrete Fourier transform length L and step size δ , the output for each microphone channel i becomes $X_i[f, t] \in R^{F \times \frac{(T+\sigma-L)}{\delta}}$, where F represents the number of frequency bins.

Feature Extraction. We developed a specialized feature extraction algorithm to isolate and enhance the direction-specific characteristics encoded by the microstructure. As presented in Eq. 3, the directional signature M_θ can be estimated using the ratio between the in-microstructure and reference microphone signals:

$$M_\theta \approx \frac{X_2[f, t]}{X_1[f, t]} \quad (4)$$

Specifically, we calculate the phase and magnitude of this ratio, which correspond to the interchannel phase differences (IPD) and interchannel level differences (ILD) – spatial cues extensively studied in binaural hearing research [7, 23]. Mathematically, these are calculated as:

$$\begin{aligned} \text{IPD}[f, t] &= \angle X_2[f, t] - \angle X_1[f, t] \\ \text{ILD}[f, t] &= 20 \log \{|X_2[f, t]|/|X_1[f, t]|\} \end{aligned} \quad (5)$$

where \angle and $|\cdot|$ denote phase and magnitude calculations of the complex number.

To facilitate neural network learning, we compute the cosine and sine transformations of the IPD, which provide a continuous representation of the circular phase information:

$$X_{feature}[f, t] = \{\cos(\text{IPD}[f, t]), \sin(\text{IPD}[f, t]), \text{ILD}[f, t]\} \quad (6)$$

We then normalize each feature across frequency bands to ensure consistent scale and improve training stability. For ILD, we apply

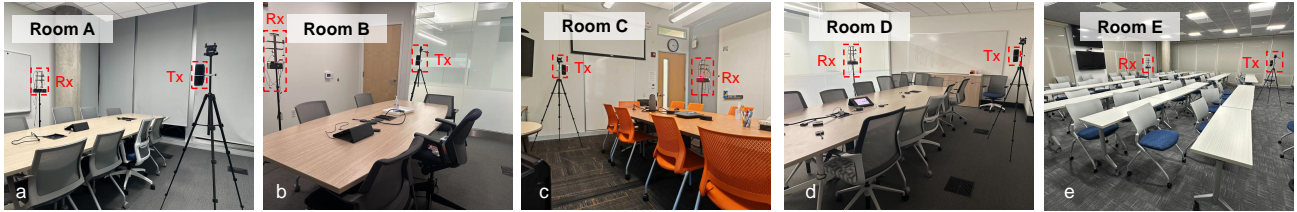


Figure 8: Real-world evaluation setup. (a–e) Five different test environments used for evaluating our system. The room dimensions are as follows (in meters): length \times width \times height. Room A, $6.1 \times 4.6 \times 3.7$ (a); Room B, $4.9 \times 3.6 \times 3.5$ (b); Room C, $6.1 \times 4.6 \times 3.7$ (c); Room D, $7.0 \times 4.9 \times 2.7$ (d); Room E, $11.5 \times 9.1 \times 2.9$ (e). In each room we play sound samples from an external speaker (model name: JBL Flip 5), and record it with multiple devices on our data capture rig.

per-frequency normalization to zero mean and unit variance, which reduces the impact of frequency-dependent gain variations inherent in the microstructure design. Similarly, while the cosine and sine IPD components are naturally bounded, normalization helps balance their influence across the spectrum where phase relationships have varying reliability at different frequencies.

The complete feature set combines the real and imaginary components of the STFT output from both microphone channels (4 channels) with our three spatial features (cosIPD, sinIPD, and ILD), resulting in 7 total feature channels. We process these through a 2D convolutional block to encode them into a representation $X \in \mathbb{R}^{c \times F \times \frac{(T+\sigma-L)}{\delta}}$, where c is the feature channel number expanded by the convolutional layer.

Angle Encoder. We represent the user’s directional selection through a 6-sector encoding system. Selected sectors are marked with 1 in a one-hot vector, while adjacent sectors receive a value of 0.25 to provide smooth spatial context. This vector passes through embedding refinement, fully connected layers, and reshaping operations to create directional embeddings that match our feature dimensions. After LayerNorm, these embeddings ($E(x)$) modulate features in each separation block through Feature-wise Linear Modulation (FiLM).

Real-time Separation Blocks. Our core processing pipeline consists of N sequential LSTM-based blocks optimized for real-time operation. Each block begins with LayerNorm and PReLU activation before using convolutional downsampling to reduce computational demands for the bidirectional LSTM. After frequency-domain processing, a deconvolution layer with skip connection restores the original dimensions. A unidirectional (causal) LSTM with a fully connected layer then processes temporal relationships, maintaining real-time performance. The FiLM layer integrates directional information by modulating features according to $E(x)$: $E_{sep} = X' * Conv1D(E(x)) + Conv1D(E(x))$, where X' represents processed features.

The final output undergoes transposed convolution and inverse STFT to generate time-domain audio. For continuous processing, we output T samples for playback while retaining σ samples for future chunk processing, enabling smooth real-time operation.

3.3 Real-world dataset

To ensure our system works well in different real-world scenarios, we augmented existing audio datasets by replaying them through a speaker in five different rooms, including meeting rooms, conference rooms and classrooms (Fig. 8).

Data sources for real-world data augmentation. We use the VCTK [54] and LibriTTS [74] datasets which contains clips of human speech. All audio clips are resampled to 24 kHz to balance audio quality and real-time requirements.

Dataset collection setup. Our data collection setup includes a JBL speaker¹ that plays sounds, and a receiver rig with two recording devices: a microphone array from MiniDSP² and a Motorola Edge smartphone with a microstructure. For our experiments, we use the smartphone’s in-line mic design with its top microphone as the reference. The receiver rig also features six LED lasers that divide the room into sectors to guide precise placement of the speaker.

To collect data, we placed the receiver in 3 random positions within each room. For each receiver spot, we positioned the transmitter in 5 different locations across all 6 sectors. At each specific transmitter-receiver pair position configuration, 6 random speech clips were played over the air. This process was repeated for 5 different rooms, yielding a total dataset of 2700 clips (6 clips \times 6 sectors \times 5 transmitter positions \times 3 receiver positions \times 5 rooms).

In software, we generated sound mixtures based on the number of target sectors. For single-target scenarios, we created 6 possible sector combinations; for two-target scenarios, 15 combinations; and for three-target scenarios, 20 combinations. This resulted in 1200 sound mixtures for each transmitter-receiver position configuration per room in single target sector scenarios, 900 mixtures for two-target sectors, and 900 mixtures for three-target sectors. We controlled the Signal-to-Noise Ratio (SNR) of signals in target sectors within a range of -5 dB to 5 dB by adjusting the scaling of sounds both inside and outside the target sectors. The mixture of reverberated signals from speakers inside the target sectors, as captured by the reference microphone, served as our ground truth.

Our complete dataset comprises 45,000 mixtures recorded across 5 different rooms. For evaluation, we employed leave-one-out validation [66], where we reserve one room’s data as the testing set to ensure that all test environments remain completely unseen during training process. Additionally, we allocated 1200 samples from the remaining data for validation.

Training methodology. During training, we maintained the smallest audio chunk at 8 ms (192 samples), with 4 ms lookahead. Accordingly, we configure the STFT and iSTFT window size as 288 samples with a shift length of 192. For input signals, we apply zero padding with a size of 96 at the signal end.

¹<https://www.jbl.com/bluetooth-speakers/JBL+FLIP+5-.html>

²<https://www.minidsp.com/products/usb-audio-interface/uma-8-microphone-array>

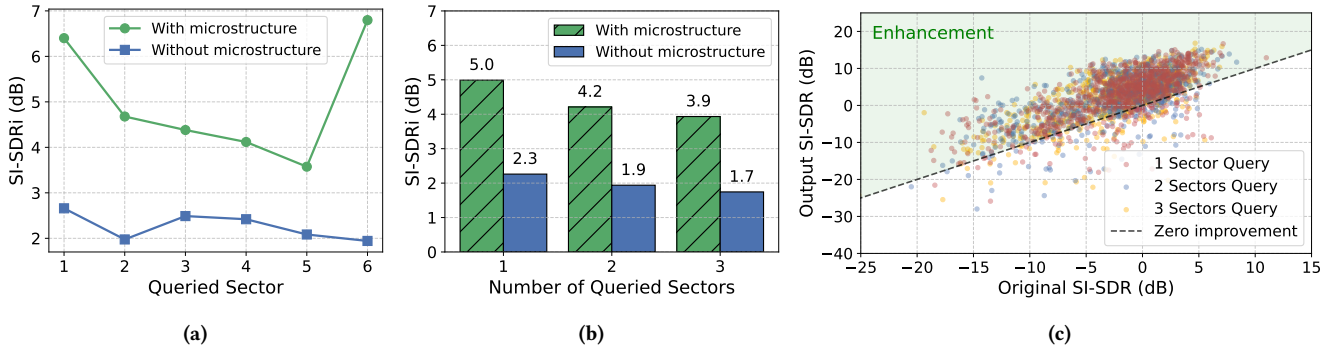


Figure 9: System performance compared to different baselines and by selected sector. (a) Effect of selected sector index on SI-SDR improvement, with and without microstructure. (b) SI-SDR improvement with and without microstructure, as a function of the number of simultaneously selected sectors. (c) Input vs. output SI-SDR of our model across all samples, grouped by 1-sector, 2-sector, and 3-sector selections. Points above the dashed line indicate cases where SI-SDR improved.

We apply a loss function based on the negative SI-SDR from asteriod package [37], defined as follows:

$$\mathcal{L}_{\text{SI-SDR}} = \begin{cases} \lambda \|\hat{s} - s\|_1 & \text{no speakers in target area} \\ -10 \log \left[\frac{\|\alpha \cdot s\|^2}{\|\alpha \cdot \hat{s}\|^2} \right] & \text{otherwise} \end{cases} \quad (7)$$

Here s is the target clean sound, \hat{s} is the output sound from the network, $\|\cdot\|_1$ is the L1-norm, and $\lambda = 50$ is a weighting factor, α can be calculated by $\alpha = \frac{\hat{s}^T s}{\|\hat{s}\|^2}$. We trained all models for 150 epochs, and apply Adam optimizer [28] with an initial learning rate as $5e-3$. The learning rate was increased from $5e-4$ to $5e-3$ over 10 epochs, held constant for 20 epochs, and then reduced by 0.95 every 2 epochs. We also applied data augmentation [65], including Time Shift, Time Stretch, Frequency Mask and Gain Perturbation during training, with a probability of 30% for each augmentation methods.

4 RESULTS

4.1 Model results

For our evaluation, we began by using the real-world datasets (Fig. 8) collected in rooms B-E for training and validation, while testing on data from room A. We further present cross-room evaluation results at the end of the section. In all our evaluations, we use data from the in-line mic version of our system.

System performance across different sectors. We measured the SI-SDR across each of the six sectors in two conditions: before applying the acoustic microstructure and after applying it, with only a single sector selected in both cases. As shown in Fig. 9a, applying the microstructure consistently achieve higher SI-SDR improvement (SI-SDRi) across all sectors (range: 3.6–6.8 dB; mean: 4.5 dB). Interestingly, we found that performance varies across sectors due to the non-uniform distribution of holes in the microstructure. Specifically, sector 1 and 6 achieve an SI-SDRi of ~ 6 -7 dB, while sector 4 and 5 achieve around ~ 4 dB. This variation is consistent with the characterization of the microstructure’s spatial diversity for different angles as shown in Fig. 6, which shows that sectors 1 and 6 correspond to angles with higher spatial diversity, while sectors 3 to 5 exhibit reduced diversity. This characteristic

can be leveraged in real-world use where users can rotate the device such that the target speaker is contained by sector 1 or 6 to achieve better directional filtering performance.

Effect of number of selected sectors. As our model is designed to support simultaneous selection of up to three sectors, we conducted a comprehensive evaluation of system performance across all possible sector combinations. This includes evaluating all individual sector (1-sector selection), all possible pairs of sectors (2-sector combinations), and all possible triplets of sectors (3-sector combinations). Each configuration was evaluated both with and without the acoustic microstructure. Our results in Fig. 9b reveal two key trends. First, the microstructure-enabled system consistently outperforms the baseline without the microstructure, regardless of selected number. When a single sector is selected, our system achieves a SI-SDRi of 5.0 dB, compared to 2.3 dB for the baseline. With two sectors selected, performance drops slightly to 4.2 dB, but still maintaining an advantage over the baseline of 1.9 dB. When three sectors are selected, the SI-SDRi with the microstructure is 3.9 dB which is greater than the baseline’s 1.7 dB. The second trend is that SI-SDRi decreases as the number of selected sectors increases for both systems. This is expected as extracting speech from multiple directions becomes more challenging when the spatial geometry of the selected region becomes more complex.

Fig. 9c shows the relationship between the input SI-SDR of the speech samples in our dataset and the output SI-SDR after processing with our model when 1, 2, or 3 sectors are selected. The diagonal dashed line represents zero improvement, where the output SI-SDR equals the input. Points above this line indicate enhanced speech quality after processing. As evident from the figure, the vast majority of our test samples (86.6%) demonstrate positive enhancement, with output SI-SDR values consistently higher than their original values. Notably, the one-sector selection configuration (represented by red dots) shows the fewest samples (9.9%) falling below the zero-improvement line compared to two- and three-sector selections (15.2% and 16.3%, respectively), confirming our earlier observation

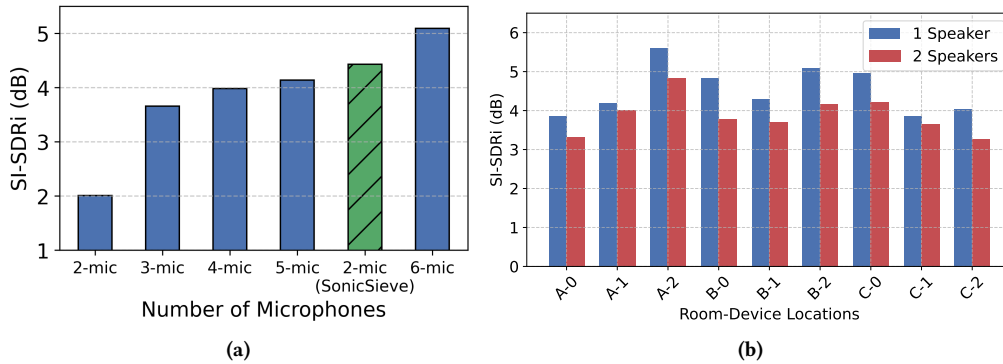


Figure 10: Stratified analysis by system variables. (a) Comparison of SI-SDR improvement across microphone arrays of varying sizes versus our *SonicSieve* system. (b) Average SI-SDR improvement across the 3 rooms (Room A, B, C) in our dataset, computed from 3 random locations (location 0, 1, 2) per room. Results are categorized by scenarios with 1 or 2 target speakers and averaged over 3000 samples per location.

that the task becomes more challenging as the number of selected sectors increases.

Comparison against microphone array. We compared the end-to-end performance of *SonicSieve* against a conventional microphone array (UMA-8 USB mic array V2.0) as a baseline. For this baseline, we leveraged 2 to 6 channels from the array and trained separate neural networks for each configuration. All baseline models were trained on the same dataset with the same architecture as *SonicSieve*, except for minor modifications to accommodate the varying number of input channels.

Fig. 10a shows the SI-SDRi, computed as the difference in SI-SDR between the sound mixture at the reference microphone and the enhanced speech output from the model. As the number of microphone channels increases from 2 to 6, SI-SDRi improves from 2.1 dB to 5.1 dB, due to the increased spatial diversity. *SonicSieve* achieves an SI-SDRi of 4.4 dB, outperforming the 5-microphone configuration (4.1 dB), and approaching the performance of the 6-microphone configuration (5.1 dB), demonstrating the effectiveness of our whole system.

Generalization across real-world environments. The previous results were developed using datasets from Rooms B–E and evaluated in Room A. To further evaluate generalizability of *SonicSieve* across environments, we conducted leave-one-room-out cross-validation for Rooms B and C. Rooms D and E were excluded from this analysis due to data collection inconsistencies in the data collection procedure (with portions of data missing). Fig. 10b presents the SI-SDRi performance across various device locations in different rooms, with each label indicating the test room (A, B, or C) and device position (0, 1, or 2) within that room. For single-speaker scenarios (blue bars), our system achieves consistent performance across all test conditions, with SI-SDRi values ranging from 3.9 to 5.7 dB. The highest performance is observed at location A-2 (5.7 dB), while the lowest occurs at C-1 (3.9 dB). Similarly, for two-speaker scenarios (red hatched bars), our system maintains stable performance across all environments, with SI-SDRi values between 3.3 and 4.8 dB. The highest performance is observed at location A-2 (4.8 dB), while the lowest occurs at C-2 (3.3 dB).

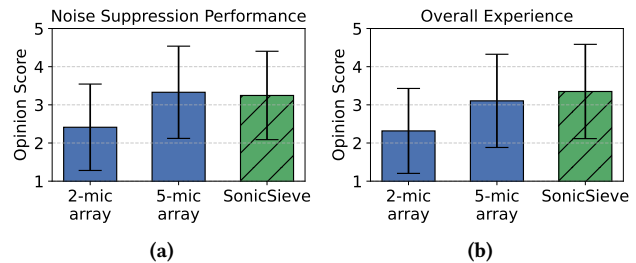


Figure 11: User study measuring listening experience via mean opinion scores: (a) audibility of interfering speakers and background noise, (b) overall listening quality.

Effect of sector resolution. Although our model is mainly trained in 6 sector cases (30 degree resolution), we conducted evaluation on how the resolution affects model performance. We compared performance between 6 sectors and 9 sectors using simulation in Pyroomacoustics [44]. With one speaker in the target sectors, *SonicSieve* achieves 7.4 dB improvement in the 9 sector case and 7.9 dB improvement in the 6 sector case. With two speakers in the target sectors, *SonicSieve* achieves 5.0 dB improvement in the 9 sector case and 5.6 dB improvement in the 6 sector case. This demonstrates that even with more sectors and a more challenging task, *SonicSieve* still achieves good performance.

Model Latency. We evaluated the latency of our directional sound extraction neural network on a variety of different smartphones models: Samsung Galaxy S21, Google Pixel 7, and Motorola Edge 2024. To do this, we exported our PyTorch model to an ONNX model that could be run on these mobile devices. We used an audio chunk size of 8 ms, which we used in our main evaluations. We ran the model for 1000 iterations and obtained mean and standard deviation latencies ranging from 4.5 ± 0.2 to 7.2 ± 0.2 ms across the phone models which is less than the 8 ms requirements needed for real-time execution.

4.2 Subjective user evaluation of audio quality

While objective metrics like SI-SDR provide valuable quantitative assessment, they cannot fully capture the perceptual quality of

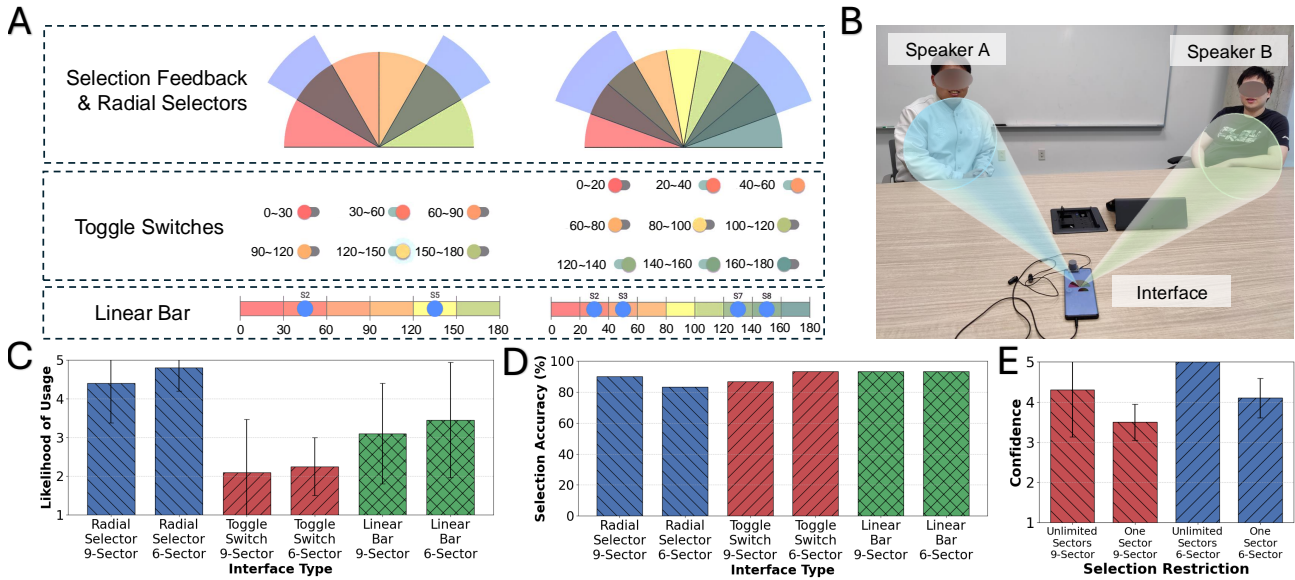


Figure 12: User interfaces for directional speech extraction. (a) Users can select the desired sector(s) using radial selectors, toggle switches or buttons on a linear bar. (b) UI evaluation setup where participants had to select one or both speakers in different scenarios. (c) Selection accuracy results for containing the target speaker. (d) Mean opinion scores for each UI. (e) Subjective confidence scores for accurately selecting target speaker(s).

speech enhancement systems in real-world scenarios. To evaluate the actual listening experience, we conduct a user study to complement our objective measurements. We randomly select 12 generated audio samples from our test set collected from Room A. The selected audio contains one target speech and 1-2 interfering sources (undesired speech or other sound). Each sample is processed by three systems: the 2-channel microphone array (baseline), 5-channel microphone array, and our proposed *SonicSieve*. 20 participants (14 males and 6 females) with an average age of 24 years were recruited for the listening test. The evaluation protocol consisted of three steps: (1) listening to the noisy audio mixture, (2) listening to the clean target speaker audio as reference, and (3) listening to the three processed outputs presented in random order to avoid position bias. Participants were asked to rate each processed audio sample on two criteria using 5-point scales:

- (1) Noise Suppression Performance: *How intrusive/noticeable were the interfering speakers and background noises? (1 – Very intrusive to 5 – Not noticeable)*
- (2) Overall Experience: *If the goal is to focus on the target speaker, how was your overall experience? (1 – Very intrusive to 5 – Not noticeable)*

As shown in Fig. 11, both *SonicSieve* and the 5-channel microphone array significantly outperform the 2-channel microphone baseline in subjective evaluations. For noise suppression performance (Fig. 11a), *SonicSieve* achieved a Mean Opinion Score (MOS) of 3.25 ± 1.16 , comparable to the 5-microphone array’s 3.33 ± 1.21 , despite using fewer microphones. Statistical analysis using a Student’s t-test indicated that the difference was not statistically significant ($t = 0.77, p = 0.44; \alpha = 0.05$). The overall listening experience (Fig. 11b) shows that *SonicSieve* outperforms the 5-microphone array (3.35 ± 1.23 vs. $3.10 \pm 1.22, t = -2.19, p = 0.03; \alpha = 0.05$). This

statistical significance confirms that participants consistently preferred *SonicSieve*’s performance in real-world listening scenarios.

4.3 User Interface

Finally, we consider how users can interact with their smartphone to select the desired direction. We designed and evaluated three user interfaces on Android (Fig. 12a). All interfaces display the selected direction on a semicircle. Users can make directional selections using 1) *Radial Selectors* by directly selecting the desired sector on the semicircle, 2) *Toggle Switches* by toggling switches labeled with angular ranges (e.g. $0 - 30^\circ, 30 - 60^\circ$ etc.), or a 3) *Linear Bar* by selecting buttons arranged linearly across the screen and labeled with angular ranges. We also investigated how sector granularity affects usability by evaluating configurations with 6 sectors (30° each) and 9 sectors (20° each) for all three UIs.

We conducted a user study across 10 participants in a conference room, with one participant and two experimenters (Fig. 12b). For each interface, the participant completed three directional selection tasks: specifically they were tasked with selecting the first experimenter (A), the second experimenter (B), and both experimenters (A+B). During each of the three tasks, experimenters positioned themselves at different predetermined locations. The positions of the experimenters were consistent across all UI evaluations to ensure fair comparisons could be made. However, within each UI the order of tasks was randomized to minimize learning effects. Participants were instructed to select any number of sectors they felt would be needed to include the target speaker(s). We evaluated interface usability through three measurements:

Selection Accuracy. We assessed whether users correctly included the target speaker(s) (Fig. 12c). In the 6-sector condition, *Toggle*



Figure 13: Applications of SonicSieve. (a–d) Our system can be physically connected to various computing devices with a microphone jack including smartphones, handheld digital voice recorders, tablets, and laptops. (e–h) *SonicSieve* can be used in various application scenarios including (e) Transcribing a presentation with speaker attribution. (f) Conducting a remote meeting by a noisy park. (g) Recording a podcast without specialized soundproof booths. (h) Interacting with an AI voice assistant in a noisy restaurant.

Switches and *Linear Bar* performed equally well (93.3%), while *Radial Selectors* exhibited the lowest accuracy (83.3%). For 9-sector condition, *Linear Bar* (93.3%) outperformed *Radial Selectors* (90.0%), with *Toggle Switches* showing the worst performance (86.7%). These results show that *Linear Bar* is the most effective interface in terms of selection accuracy, likely because it provides users with strong spatial references as well as precise numerical markers.

Interface Preference. We asked participants to rate their likelihood of using each UI on a 5-point scale (1 = extremely unlikely, 5 = extremely likely) (Fig. 12d). Participants rated *Radial Selectors* highest in both 6- and 9-sector settings (4.8 ± 0.6 and 4.4 ± 1.0), followed by *Linear Bar* (3.5 ± 1.5 and 3.1 ± 1.3), with *Toggle Switches* rated lowest (2.3 ± 0.8 and 2.1 ± 1.4). Users preferred *Radial Selectors* for its intuitive spatial mapping, while *Toggle Switches*' lack of spatial correspondence led to repeated selection attempts and lower scores. Ratings were consistently higher for 6-sector interfaces, which users found easier and less error-prone to accidental selection of adjacent sectors. While most users prioritized ease of use, a few preferred *Toggle Switches* or *Linear Bar* in the 9-sector setting as it gave them greater sense precision in their selections.

Selection Confidence. We assessed users' confidence in their selections under two conditions: when they were restricted to selecting only one sector versus when they could select multiple sectors (Fig. 12e). We performed a within-subjects experiments where we requested users to rate their selection confidence between 1 and 5 and allowed them to use their preferred UI. In the 9-sector configuration, confidence decreased from 4.3 ± 1.2 when multiple sectors were allowed to 3.5 ± 0.5 when restricted to a single sector. A similar trend was observed in the 6-sector configuration, where confidence dropped from 5.0 ± 0.0 to 4.1 ± 0.5 under the single-sector condition. These results suggest that users consistently preferred to select multiple sectors, which increased their confidence at identifying the target experimenter. Furthermore, the 6-sector layout led to higher overall confidence, likely because it reduced user concerns about the precision required for accurate selection.

5 LIMITATIONS AND DISCUSSION

Source separation within a sector. Our system currently performs spatial filtering along predefined directional sectors and produces a mixture of all sounds it. This can be undesirable when multiple speakers are close to each other and fall within the same sector. Future extensions of this work could address this limitation in two ways: (1) A low-latency speech separation framework [24, 25, 71] can be applied after directional speech extraction, using permutation-invariant training to separate multiple speakers. (2) More fine-grained separation can be performed in the spatial domain by building on techniques for region-customizable sound extraction [23] to spatially isolate the target speaker.

Speaker mobility. Our current system is designed primarily for scenarios where the speaker remains relatively stationary such as in meetings. If the speaker moves, the user is expected to manually update the target sector. However, this is not a fundamental limitation of our neural network approach. Future extensions of the model could be explicitly trained to estimate the direction of arrival (DoA) for multiple speakers [17, 60, 63], and enable dynamic conditioning of the directional speech extraction network.

Audio playback. While our current system is focused on speech transcription and remote streaming, our model's processing latency is low enough for real-time, on-device playback of the extracted audio to users. With a smartphone-native design (Fig. 13a), playback can be achieved using noise-canceling headphones, similar to prior AI-enabled acoustic systems [11, 55], which leverage both passive and active noise cancellation to suppress ambient sounds and deliver clear playback of the extracted sounds.

A limitation of the current in-line microphone setup is the close proximity of the mic to the earphones, resulting in insufficient wire length to comfortably reach a user's ears when the smartphone is placed on a table. This can be addressed in two ways. First, a custom but low-cost headphone could be designed with the in-line mic positioned farther from the speakers, allowing the phone to remain on a surface while maintaining sufficient wire length. Alternatively,

wireless headphones could be used for playback by integrating the acoustic microstructure onto one of the outward-facing microphones typically used for noise cancellation. This approach is likely possible as modern headphones often include dual outward-facing microphones for noise cancellation, and low-power GPUs are becoming integrated into wearable devices [1, 48].

References

- [1] 2025. GPU-WEAR, Ultra-low power heterogeneous Graphics Processing Units for Wearable/IoT devices. <https://cordis.europa.eu/project/id/717850>
- [2] Inkyu An, Youngsun Kwon, and Sung-eui Yoon. 2022. Diffraction- and Reflection-Aware Multiple Sound Source Localization. *IEEE Transactions on Robotics* 38, 3 (2022), 1925–1944. doi:10.1109/TRO.2021.3118966
- [3] Inkyu An, Myungbae Son, Dinesh Manocha, and Sung-Eui Yoon. 2018. Reflection-Aware Sound Source Localization. In *2018 IEEE International Conference on Robotics and Automation (ICRA)*. 66–73. doi:10.1109/ICRA.2018.8461268
- [4] Arun Arjunan, Ahmad Baroutaji, John Robinson, Aaron Vance, and Abul Arafat. 2024. Acoustic metamaterials for sound absorption and insulation in buildings. *Building and Environment* 251 (2024), 111250.
- [5] Yang Bai, Nakul Garg, and Nirupam Roy. 2022. Spidr: Ultra-low-power acoustic spatial sensing for micro-robot navigation. In *Proceedings of the 20th Annual International Conference on Mobile Systems, Applications and Services*. 99–113.
- [6] Axel Berg, Jens Gulin, Mark O’Connor, Chuteng Zhou, Karl Åström, and Magnus Oskarsson. 2024. wav2pos: Sound Source Localization using Masked Autoencoders. In *2024 14th International Conference on Indoor Positioning and Indoor Navigation (IPIN)*.
- [7] Jens Blauert. 1997. *Spatial hearing: the psychophysics of human sound localization*. MIT press.
- [8] Andrew Brughera, Jason Mikiel-Hunter, Mathias Dietz, and David McAlpine. 2019. Brainstem biophysics contribute to sound-source localisation in reverberant scenes. *bioRxiv* (2019). doi:10.1101/694356
- [9] Gaoshuai Cao, Kuang Yuan, Jie Xiong, Panlong Yang, Yubo Yan, Hao Zhou, and Xiang-Yang Li. 2020. Earphonetrack: involving earphones into the ecosystem of acoustic motion tracking. In *Proceedings of the 18th Conference on Embedded Networked Sensor Systems*. 95–108.
- [10] Ishan Chatterjee, Maruchi Kim, Vivek Jayaram, Shyamnath Gollakota, Ira Kemelmacher-Shlizerman, Shwetak Patel, and Steven M Seitz. 2022. ClearBuds: wireless binaural earbuds for learning-based speech enhancement. In *Proceedings of the 20th Annual International Conference on Mobile Systems, Applications and Services*. 384–396.
- [11] Tuocho Chen, Malek Itani, Sefik Emre Eskimez, Takuya Yoshioka, and Shyamnath Gollakota. 2024. Hearable devices with sound bubbles. *Nature Electronics* (2024), 1–12.
- [12] Zhuo Chen, Xiong Xiao, Takuya Yoshioka, Hakan Erdogan, Jinyu Li, and Yifan Gong. 2018. Multi-channel overlapped speech recognition with location guided speech extraction network. In *2018 IEEE Spoken Language Technology Workshop (SLT)*. IEEE, 558–565.
- [13] Ming-An Chung, Hung-Chi Chou, and Chia-Wei Lin. 2022. Sound Localization Based on Acoustic Source Using Multiple Microphone Array in an Indoor Environment. *Electronics* 11 (03 2022), 890. doi:10.3390/electronics11060890
- [14] Roger B Coles and Anna Guppy. 1988. Directional hearing in the barn owl (*Tyto alba*). *Journal of Comparative Physiology A* 163, 1 (1988), 117–133.
- [15] Tobias Cord-Landwehr, Christoph Boeddeker, Thilo Von Neumann, Cătălin Zorilă, Rama Doddipatla, and Reinhold Haeb-Umbach. 2022. Monaural source separation: From anechoic to reverberant environments. In *2022 international workshop on acoustic signal enhancement (IWAENC)*. IEEE, 1–5.
- [16] Dhvani Desai and Ninad Mehendale. 2022. A Review on Sound Source Localization Systems. *Archives of Computational Methods in Engineering* 29 (05 2022), doi:10.1007/s11831-022-09747-2
- [17] Nilanjan Dey and Amira S Ashour. 2018. *Direction of arrival estimation and localization of multi-speech sources*. Springer.
- [18] Thomas Dupont, Philippe Leclaire, Raymond Panneton, and Olga Umnova. 2018. A microstructure material design for low frequency sound absorption. *Applied Acoustics* 136 (2018), 86–93.
- [19] Andrew Francl and Josh McDermott. 2022. Deep neural network models of sound localization reveal how perception is adapted to real-world environments. *Nature Human Behaviour* 6 (01 2022), 111–133. doi:10.1038/s41562-021-01244-z
- [20] Nakul Garg, Yang Bai, and Nirupam Roy. 2021. Owllet: Enabling spatial information in ubiquitous acoustic devices. In *Proceedings of the 19th Annual International Conference on Mobile Systems, Applications, and Services*. 255–268.
- [21] Nikolay D Gaubitch, Jorge Martinez, W Bastiaan Kleijn, and Richard Heusdens. 2014. On near-field beamforming with smartphone-based ad-hoc microphone arrays. In *2014 14th International Workshop on Acoustic Signal Enhancement (IWAENC)*. IEEE, 94–98.
- [22] Rongzhi Gu, Lianwu Chen, Shi-Xiong Zhang, Jimeng Zheng, Yong Xu, Meng Yu, Dan Su, Yuexian Zou, and Dong Yu. 2019. Neural Spatial Filter: Target Speaker Speech Separation Assisted with Directional Information.. In *Interspeech*. 4290–4294.
- [23] Rongzhi Gu and Yi Luo. 2024. Rezero: Region-customizable sound extraction. *IEEE/ACM Transactions on Audio, Speech, and Language Processing* (2024).
- [24] Rongzhi Gu, Shi-Xiong Zhang, Meng Yu, and Dong Yu. 2021. 3d spatial features for multi-channel target speech separation. In *2021 IEEE Automatic Speech Recognition and Understanding Workshop (ASRU)*. IEEE, 996–1002.
- [25] Rongzhi Gu, Shi-Xiong Zhang, Yuexian Zou, and Dong Yu. 2022. Towards unified all-neural beamforming for time and frequency domain speech separation. *IEEE/ACM Transactions on Audio, Speech, and Language Processing* 31 (2022), 849–862.
- [26] Rongzhi Gu and Yuexian Zou. 2020. Temporal-spatial neural filter: Direction informed end-to-end multi-channel target speech separation. *arXiv preprint arXiv:2001.00391* (2020).
- [27] Teerapat Jenrungrot, Vivek Jayaram, Steve Seitz, and Ira Kemelmacher-Shlizerman. 2020. The cone of silence: Speech separation by localization. *Advances in Neural Information Processing Systems* 33 (2020), 20925–20938.
- [28] Diederik P Kingma and Jimmy Ba. 2014. Adam: A method for stochastic optimization. *arXiv preprint arXiv:1412.6980* (2014).
- [29] Anton Kovalyov, Kashyap Patel, and Issa Panahi. 2023. Dsenet: Directional signal extraction network for hearing improvement on edge devices. *IEEE Access* 11 (2023), 4350–4358.
- [30] Abdullah Küçük, Anshuman Ganguly, Yiya Hao, and Issa MS Panahi. 2019. Real-time convolutional neural network-based speech source localization on smartphone. *IEEE Access* 7 (2019), 169969–169978.
- [31] Milind N Kunchur. 2023. The human auditory system and audio. *Applied Acoustics* 211 (2023), 109507.
- [32] Dingzeyu Li, David IW Levin, Wojciech Matusik, and Changxi Zheng. 2016. Acoustic voxels: Computational optimization of modular acoustic filters. *ACM Transactions on Graphics (TOG)* 35, 4 (2016), 1–12.
- [33] Guinan Li, Xue Bao, and Zhi Wang. 2017. The design and implementation of a smartphone-based acoustic array system for DOA estimation. In *2017 36th Chinese Control Conference (CCC)*. IEEE, 5416–5423.
- [34] Xin Li, Yilin Wang, Zhengkun Ye, Yan Wang, and Yingying Chen. 2023. Earcase: Sound source localization leveraging mini acoustic structure equipped phone cases for hearing-challenged people. In *Proceedings of the Twenty-fourth International Symposium on Theory, Algorithmic Foundations, and Protocol Design for Mobile Networks and Mobile Computing*. 240–249.
- [35] Thi Ngoc Tho Nguyen, Karn N Watcharasupat, Ngoc Khanh Nguyen, Douglas L Jones, and Woon-Seng Gan. 2022. Salsa: Spatial cue-augmented log-spectrogram features for polyphonic sound event localization and detection. *IEEE/ACM Transactions on Audio, Speech, and Language Processing* 30 (2022), 1749–1762.
- [36] Ashutosh Pandey, Sanha Lee, Juan Azcarreta, Daniel Wong, and Buye Xu. 2024. All Neural Low-latency Directional Speech Extraction. *arXiv preprint arXiv:2407.04879* (2024).
- [37] Manuel Pariente, Samuele Cornell, Joris Cosentino, Sunit Sivasankaran, Efthymios Tzinis, Jens Heitkaemper, Michel Olvera, Fabian-Robert Stöter, Mathieu Hu, Juan M Martin-Doñas, et al. 2020. Asteroid: the PyTorch-based audio source separation toolkit for researchers. *arXiv preprint arXiv:2005.04132* (2020).
- [38] Santiago Pascual, Antonio Bonafonte, and Joan Serra. 2017. SEGAN: Speech enhancement generative adversarial network. *arXiv preprint arXiv:1703.09452* (2017).
- [39] KS Peat. 1994. A first approximation to the effects of mean flow on sound propagation through cylindrical capillary tubes. *Journal of sound and vibration* 175, 4 (1994), 475–489.
- [40] Chunyi Peng, Guobin Shen, Yongguang Zhang, Yanlin Li, and Kun Tan. 2007. Bleepbeep: a high accuracy acoustic ranging system using cots mobile devices. In *Proceedings of the 5th international conference on Embedded networked sensor systems*. 1–14.
- [41] Allan D Pierce. 1974. Diffraction of sound around corners and over wide barriers. *The Journal of the Acoustical Society of America* 55, 5 (1974), 941–955.
- [42] Kaizhi Qian, Yang Zhang, Shiyu Chang, Xuesong Yang, Dinei Florencio, and Mark Hasegawa-Johnson. 2018. Deep learning based speech beamforming. In *2018 IEEE International Conference on Acoustics, Speech and Signal Processing (ICASSP)*. IEEE, 5389–5393.
- [43] Ashutosh Saxena and Andrew Y. Ng. 2009. Learning sound location from a single microphone. In *2009 IEEE International Conference on Robotics and Automation*. 1737–1742. doi:10.1109/ROBOT.2009.5152861
- [44] Robin Scheibler, Eric Bezzam, and Ivan Dokmanić. 2018. Pyroomacoustics: A python package for audio room simulation and array processing algorithms. In *2018 IEEE international conference on acoustics, speech and signal processing (ICASSP)*. IEEE, 351–355.
- [45] Sheng Shen, Daguang Chen, Yu-Lin Wei, Zhijian Yang, and Romit Roy Choudhury. 2020. Voice localization using nearby wall reflections. In *Proceedings of the 26th Annual International Conference on Mobile Computing and Networking*. 1–14.
- [46] Kazuki Shimada, Yuichiro Koyama, Naoya Takahashi, Shusuke Takahashi, and Yuki Mitsufuji. 2021. ACCDOA: Activity-coupled cartesian direction of arrival representation for sound event localization and detection. In *ICASSP 2021-2021*

- IEEE international conference on acoustics, speech and signal processing (ICASSP)*. IEEE, 915–919.
- [47] Sanjib Sur, Teng Wei, and Xinyu Zhang. 2014. Autodirective audio capturing through a synchronized smartphone array. In *Proceedings of the 12th annual international conference on Mobile systems, applications, and services*. 28–41.
- [48] Thierry Tambe, En-Yu Yang, Glenn G Ko, Yuji Chai, Coleman Hooper, Marco Donato, Paul N Whatmough, Alexander M Rush, David Brooks, and Gu-Yeon Wei. 2022. A 16-nm soc for noise-robust speech and nlp edge ai inference with bayesian sound source separation and attention-based dnns. *IEEE Journal of Solid-State Circuits* 58, 2 (2022), 569–581.
- [49] PK Tang and WA Sirignano. 1973. Theory of a generalized Helmholtz resonator. *Journal of Sound and Vibration* 26, 2 (1973), 247–262.
- [50] Kristina Tesch and Timo Gerkmann. 2022. Insights into deep non-linear filters for improved multi-channel speech enhancement. *IEEE/ACM Transactions on Audio, Speech, and Language Processing* 31 (2022), 563–575.
- [51] H Tijdeman. 1975. On the propagation of sound waves in cylindrical tubes. *Journal of Sound and Vibration* 39, 1 (1975), 1–33.
- [52] Serkan Tokgöz, Anton Kovalyov, and Issa Panahi. 2020. Real-time estimation of direction of arrival of speech source using three microphones. In *2020 IEEE Workshop on Signal Processing Systems (SiPS)*. IEEE, 1–5.
- [53] John Van Opstal. 2016. *The auditory system and human sound-localization behavior*. Academic Press.
- [54] Christophe Veaux, Junichi Yamagishi, Kirsten MacDonald, et al. 2017. CSTR VCTK corpus: English multi-speaker corpus for CSTR voice cloning toolkit. *University of Edinburgh. The Centre for Speech Technology Research (CSTR)* 6 (2017), 15.
- [55] Bandhav Veluri, Malek Itani, Justin Chan, Takuya Yoshioka, and Shyamnath Gollakota. 2023. Semantic hearing: Programming acoustic scenes with binaural hearables. In *Proceedings of the 36th Annual ACM Symposium on User Interface Software and Technology*. 1–15.
- [56] Bandhav Veluri, Malek Itani, Tuochao Chen, Takuya Yoshioka, and Shyamnath Gollakota. 2024. Look Once to Hear: Target Speech Hearing with Noisy Examples. In *Proceedings of the CHI Conference on Human Factors in Computing Systems*. 1–16.
- [57] Anran Wang, Maruchi Kim, Hao Zhang, and Shyamnath Gollakota. 2022. Hybrid neural networks for on-device directional hearing. In *Proceedings of the AAAI Conference on Artificial Intelligence*, Vol. 36. 11421–11430.
- [58] Anran Wang, Dan Nguyen, Arun R Sridhar, and Shyamnath Gollakota. 2021. Using smart speakers to contactlessly monitor heart rhythms. *Communications biology* 4, 1 (2021), 319.
- [59] Anran Wang, Jacob E Sunshine, and Shyamnath Gollakota. 2019. Contactless infant monitoring using white noise. In *The 25th Annual International Conference on Mobile Computing and Networking*. 1–16.
- [60] Rui Wang, Li Li, and Tomoki Toda. 2024. Dual-Channel Target Speaker Extraction Based on Conditional Variational Autoencoder and Directional Information. *IEEE/ACM Transactions on Audio, Speech, and Language Processing* 32 (2024), 1968–1979. doi:10.1109/TASLP.2024.3376154
- [61] Zeyu Wang, Xiyuxing Zhang, Ruotong Yu, Yuntao Wang, Kenneth Christoffer-son, Jingru Zhang, Alex Mariakakis, and Yuanchun Shi. 2024. DreamCatcher: A Wearer-aware Multi-modal Sleep Event Dataset Based on Earables in Non-restrictive Environments. In *Advances in Neural Information Processing Systems*, A. Globerson, L. Mackey, D. Belgrave, A. Fan, U. Paquet, J. Tomczak, and C. Zhang (Eds.), Vol. 37. Curran Associates, Inc., 85155–85178. https://proceedings.neurips.cc/paper_files/paper/2024/file/9ab8bb568825d49ce31aa87b7e2f4ad7-Paper-Datasets_and_Benchmarks_Track.pdf
- [62] Zhong-Qiu Wang, Samuele Cornell, Shukjae Choi, Younglo Lee, Byeong-Yeol Kim, and Shinji Watanabe. 2023. TF-GridNet: Integrating full-and sub-band modeling for speech separation. *IEEE/ACM Transactions on Audio, Speech, and Language Processing* 31 (2023), 3221–3236.
- [63] Zhong-Qiu Wang, Xueliang Zhang, and DeLiang Wang. 2019. Robust Speaker Localization Guided by Deep Learning-Based Time-Frequency Masking. *IEEE/ACM Transactions on Audio, Speech, and Language Processing* 27, 1 (2019), 178–188. doi:10.1109/TASLP.2018.2876169
- [64] Julian Wechsler, Srikanth Raj Chetupalli, Wolfgang Mack, and Emanuel A. P. Habets. 2023. Multi-Microphone Speaker Separation by Spatial Regions. arXiv:2303.07143 [eess.AS] <https://arxiv.org/abs/2303.07143>
- [65] Shengyun Wei, Shun Zou, Feifan Liao, and weimin lang. 2020. A Comparison on Data Augmentation Methods Based on Deep Learning for Audio Classification. *Journal of Physics: Conference Series* 1453, 1 (jan 2020), 012085. doi:10.1088/1742-6596/1453/1/012085
- [66] Tzu-Tsung Wong. 2015. Performance evaluation of classification algorithms by k-fold and leave-one-out cross validation. *Pattern recognition* 48, 9 (2015), 2839–2846.
- [67] Bo Wu, Kehuang Li, Minglei Yang, and Chin-Hui Lee. 2016. A reverberation-time-aware approach to speech dereverberation based on deep neural networks. *IEEE/ACM transactions on audio, speech, and language processing* 25, 1 (2016), 102–111.
- [68] Bosun Xie. 2013. *Head-related transfer function and virtual auditory display*. J. Ross Publishing.
- [69] Yilin Yang, Xin Li, Zhengkun Ye, Yan Wang, and Yingying Chen. 2023. BioCase: Privacy Protection via Acoustic Sensing of Finger Touches on Smartphone Case Mini-Structures. In *Proceedings of the 21st Annual International Conference on Mobile Systems, Applications and Services*. 397–409.
- [70] Yang Yang, George Sung, Shao-Fu Shih, Hakan Erdogan, Chehung Lee, and Matthias Grundmann. 2024. Binaural angular separation network. In *ICASSP 2024-2024 IEEE International Conference on Acoustics, Speech and Signal Processing (ICASSP)*. IEEE, 1201–1205.
- [71] Kuang Yuan, Shuo Han, Swarn Kumar, and Bhiksha Raj. 2024. DeWinder: Single-Channel Wind Noise Reduction using Ultrasound Sensing. In *Proc. Interspeech 2024*. 627–631.
- [72] Kuang Yuan, Mohamed Ibrahim, Yiwen Song, Guoxiang Deng, Robert A Nerone, Suwendra Vijayan, Akshay Gadre, and Swarn Kumar. 2024. ToMoBrush: Exploring Dental Health Sensing Using a Sonic Toothbrush. *Proceedings of the ACM on Interactive, Mobile, Wearable and Ubiquitous Technologies* 8, 3 (2024), 1–27.
- [73] Kuang Yuan, Dong Li, Hao Zhou, Zhehao Li, Lili Qiu, Swarn Kumar, and Jie Xiong. 2025. WindDancer: Understanding Acoustic Sensing under Ambient Airflow. *Proceedings of the ACM on Interactive, Mobile, Wearable and Ubiquitous Technologies* 9, 2 (2025).
- [74] Heiga Zen, Viet Dang, Rob Clark, Yu Zhang, Ron J Weiss, Ye Jia, Zhifeng Chen, and Yonghui Wu. 2019. Libritts: A corpus derived from librispeech for text-to-speech. *arXiv preprint arXiv:1904.02882* (2019).
- [75] Xiyuxing Zhang, Yuntao Wang, Yuxuan Han, Chen Liang, Ishan Chatterjee, Jiankai Tang, Xin Yi, Shwetak Patel, and Yuanchun Shi. 2024. The EarSAVAS Dataset: Enabling Subject-Aware Vocal Activity Sensing on Earables. *Proc. ACM Interact. Mob. Wearable Ubiquitous Technol.* 8, 2, Article 83 (May 2024), 26 pages. doi:10.1145/3659616
- [76] Xiyuxing Zhang, Yuntao Wang, Jingru Zhang, Yaqing Yang, Shwetak Patel, and Yuanchun Shi. 2023. EarCough: Enabling Continuous Subject Cough Event Detection on Hearables. In *Extended Abstracts of the 2023 CHI Conference on Human Factors in Computing Systems (Hamburg, Germany) (CHI EA '23)*. Association for Computing Machinery, New York, NY, USA, Article 94, 6 pages. doi:10.1145/3544549.3585903
- [77] Hao Zhou, Kuang Yuan, Mahanth Gowda, Lili Qiu, and Jie Xiong. 2024. Rethinking Orientation Estimation with Smartphone-equipped Ultra-wideband Chips. In *Proceedings of the 30th Annual International Conference on Mobile Computing and Networking*. 1045–1059.